Novel Er3+ doped heavy metals-oxyfluorophosphate glass as a blue emitter

Aly Saeed (aly-saeed@eru.edu.eg)
Egyptian Russian University

S. Sobaih
Egyptian Russian University

W. Abu-raia
Institute of Aviation Engineering & Technology

A. Abdelghany
Al-Azhar University

Sh. Heikel
Al-Azhar University

Research Article

Keywords: Photonic Glass, Blue Emission, Heavy Metals-Oxyfluorophosphates Glass, Er3+ ion

Posted Date: May 13th, 2021

DOI: https://doi.org/10.21203/rs.3.rs-473621/v1

Version of Record: A version of this preprint was published at Optical and Quantum Electronics on August 9th, 2021. See the published version at https://doi.org/10.1007/s11082-021-03171-9.

Novel Er^{3+} doped heavy metals-oxyfluorophosphate glass as a blue emitter

Aly Saeed[a*], S. Sobaih[a], W. A. Abu-raia[b], A. Abdelghany [c], Sh. Heikal [c]

[a]*Mathematical and Natural Science Department, Faculty of Engineering, Egyptian-Russian University, Cairo, Egypt*

[b]*Basic Science department, Institute of Aviation Engineering & Technology, Giza, Egypt*

[c]*Physics Department, Faculty of science (Girls Branch), Al-Azhar University, Cairo, Egypt*

Abstract

Developed P_2O_5-ZnO-PbO-WO_3-NaF glasses containing Er^{3+} ions were prepared by the melt/casting procedures. X-ray diffraction patterns confirmed the amorphicity of the prepared materials. The density and Fourier Transform Infrared FTIR spectroscopy showed that Er^{3+} ions play a modifier role and the studied glasses have low phonon energy. The observed decrease in the measured glass transition temperature indicates that the decrease in the bonding strength of the studied glass structure. The studied glass has a high thermal stability. Vickers microhardness results showed the weakening of the glass network. Measured UV-Vis absorption spectra exhibited several bands in the ultraviolet and visible regions. The studied glass has a high refractive index. The metallization criterion showed that the studied glasses have an insulating behavior. The metallization criterion values of the present glasses are in the range of nonlinear optical materials. Under 320 nm excitation wavelength, the studied glass generates three blue bands at 446, 457, and 473 nm. The CIE-1931 chromaticity diagram coordinates confirmed the blue emission of the prepared glass. According to the obtained results, the produced glasses have a high potential for using as efficient luminescence materials for photonic devices in the blue region.

Keywords: *Photonic Glass, Blue Emission, Heavy Metals-Oxyfluorophosphates Glass,* Er^{3+} ion

1. Introduction

Recently, photonic materials play a tremendous role in several modern devices. A high-broad category of optical instruments relies on the efficiency of light emission in a certain region of the electromagnetic spectrum [1-2]. The generation and control in the four fundamental colors of white light, blue, green, yellow, and red using the photonic materials have been investigated extensively [3-5]. Several photonic materials have been studied for various optical and electro-optical devices, among them the glass materials. Glassy materials emerged and occupied a topping rank in this field due to their various advantages like ease of fabrication, translucence, the solubility

*Corresponding Author: **aly-saeed@eru.edu.eg**

of high concentration of rare earth ions, and cost-effective production [6-7]. Phosphate is considered a superior host matrix that has good thermal stability, high transparency over the UV and visible wavelength range, and especially good solubility of rare-earth ions. Due to their properties, phosphate glasses were regarded as better hosts compared to other host glass networks [8-10].The poor chemical durability of phosphate glass is always treated by addition suitable oxides such as ZnO, MoO_3, and Al_2O_3. On the other hand, inlaying the phosphate network with ZnO improves the optical and electronic properties of phosphate glass [11-12]. Fluoride host materials have a high quantum yield of luminescence due to ionic bonds and low phonon energy of fluoride [13-14]. Heavy metals rich glass have a combination of desirable optical, mechanical, and thermal properties of its constituents. The inclusion of heavy metal ions in the glass matrices is of interest to the realization of more efficient photonic behavior in which their presence improves the efficiency of fluorescence. The addition of heavy metal oxides minimize the host phonon energy and thereby suppressing the non-radiative losses [15-16]. In view of the foregoing, heavy metal oxyfluorophosphate glasses are excellent selection as host materials for several active optical applications. Trivalent erbium ion Er^{3+} is used as a dopant in various host glasses due to its unique optical properties. The erbium ion is an ideal candidate to be used widely in photonic applications due to its rich energy levels in near infrared, visible, and ultraviolet range [17-19].

The motivation of the present work is to develop a low phonon energy of glass system incorporated with Er^{3+} ions for photonic applications. X-ray diffraction, density, FTIR, DSC, Vickers microhardness, optical absorption were measured. Many structural, thermal, and optical parameters such as mean phosphor– phosphor separation, glass stability, optical band gap, refractive index.

2.Experimental Techniques

2.1.Materials Synthesis

Proper amounts of high purity oxides and fluoride were synthesized and melted to get heavy metal oxyfluorophosphate glass containing Er^{3+} ion in the chemical formula $45P_2O_5$-25ZnO-(20-x)PbO-5WO3-5NaF-xEr_2O_3, where x in mol% is equal to 0, 1, and 2. The raw materials in the powder form were mixed thoroughly in the agate mortar and placed in a porcelain crucible for melting it in an electric furnace at 1100 °C for 2 h to obtain a homogenous bubble free liquid. During the melting period, the molten was intermittent stirring at regular intervals then quenched on a preheated stainless steel mold. The obtained glasses were annealed below the glass transition temperature to eliminate internal thermal stresses.

2.2.Measurements

The structural phase of the prepared materials was examined using X-ray diffraction mechanism [Shimadzu XD3A radiation with Cuk_{α} =1.54056 A^{o}]. Bulk density was measured at room temperature using Archimedes principle by xylene as the buoyancy liquid (0.86 g/cm^3) using the relation [20-21]

$$\rho = \frac{W_a \rho_x}{(W_a - W_b)} \qquad (1)$$

Where, W_a is the glass piece weight in air, W_b is its weight in xylene liquid, $(W_a - W_b)$ is the buoyancy and ρ_x is the density of xylene. The measured values have been conducted three times and the average was taken.

The structural units of the obtained glasses were studied by computerized FTIR spectrophotometer [JASCO FT-IR-300] using KBr as a reference material in the spectral 400 – 4000 cm^{-1}. Differential scanning calorimeter DSC measurements were carried out by TA Instruments, SDT Q600 in an open platinum pan at heating rates of 10 ℃/min up to higher than 600 C in a high-purity nitrogen atmosphere and at a flow rate 15 Psi. The test was performed to identify the characteristic temperatures such as the glass transition and onset of crystallization with accuracy ±3 (K) under non-isochronal conditions. The Vickers microhardness was measured using HMV Shimadzu microhardness tester with a load equal to 490.3 mN by a force duration of 10 second for each sample. Five randomly indentation was tested on the same smooth surface for each sample. About 2 mm glass sample thickness had been polished for UV-visible absorption spectra measurements in the range 190–1100 nm using *Jenway 6405 UV/Vis* Spectrophotometer. The photoluminescence spectra were measured using an SPEX spectrofluorimeter (Model Fluorolog-II, SPEX CertiPrep, Metuchen, NJ) in the wavelength region of 300–500 nm under 320 nm excitation wavelength with ±1.5 wavelength accuracy emitted from 150W Xenon lamb. The PL measurements were performed on the flat and smooth surface specimens.

3.Results and Discussion

3.1.Powder X-ray diffraction (XRD)

The obtained results of the X-ray diffraction patterns are exhibited in **Figure 1**. The two beaks and high noise signal in the diffraction patterns reflect the feature of non-periodic arrangement of atoms in the obtained solid materials. The showed spectra confirm the amorphous structure of the

studied materials. The X-ray diffractograms have a notable broad band due to the interplanar spacing in the glass structure.

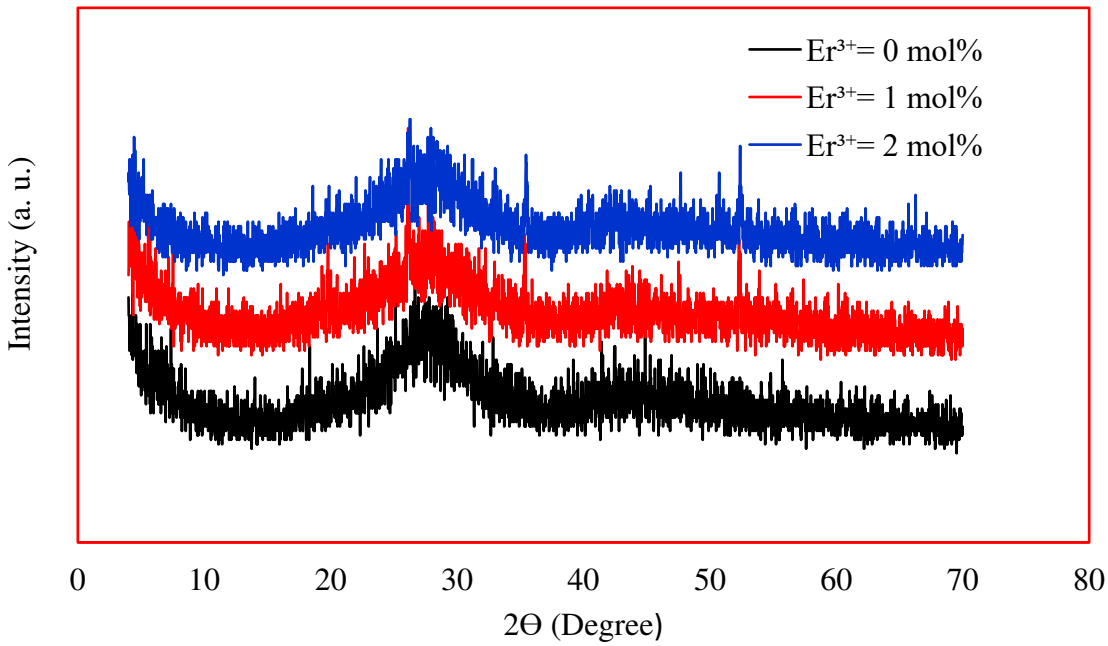

Fig 1: *X-ray diffraction patterns for the studied materials*

3.2.Density, Molar Volume, and mean phosphor– phosphor separation

The alteration of density ρ and molar volume V_m with the increase of Er^{3+} ions are shown in **Figure 2.** The Molar volume V_m (cm^3/mol) was calculated using the molecular weight M (g/mol) and the experimental density ρ_{exp} (g/cm^3) according to the formula [20-21].

$$V_m = \frac{M}{\rho} \qquad (2)$$

The results revealed diminution in density and growth in molar volume with Er^{3+} ions increment. The noticeable decrease in the density and augmentation in molar volume indicate that the inclusion of Er^{3+} ions to the proposed glass matrix create more interstitial space in the glass network. This space occurs due to the formation of non-bridging oxygens NBOs. The tangible augment of molar volume refers to Er^{3+} ions occupy the interstitial space in the present glass network, which meaning the Er^{3+} ions enter as a modifier in the studied glass network. This behavior of Er^{3+} is responsible for creating the NBOs inside the present glass structure.

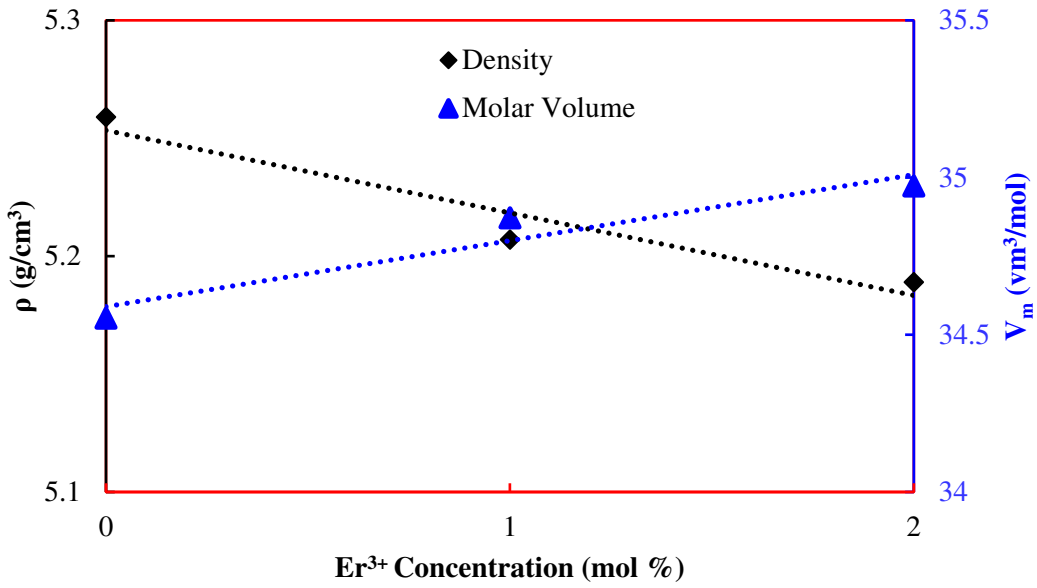

Fig 2: *The obtained results of density and molar volume of the studied glasses*

The mean phosphor – phosphor separation d_{P-P} was calculated using standard formula [21].

$$d_{P-P} = \left(\frac{V_M^P}{N_A}\right)^{\frac{1}{3}} \qquad (3)$$

$$V_M^P = \frac{V_M}{2(1 - X_P)}$$

where the volume V_M^P corresponds to the volume that contains one mole of phosphor within the given structure and X_P molar fraction of P_2O_5, and N_A Avogadro's number.

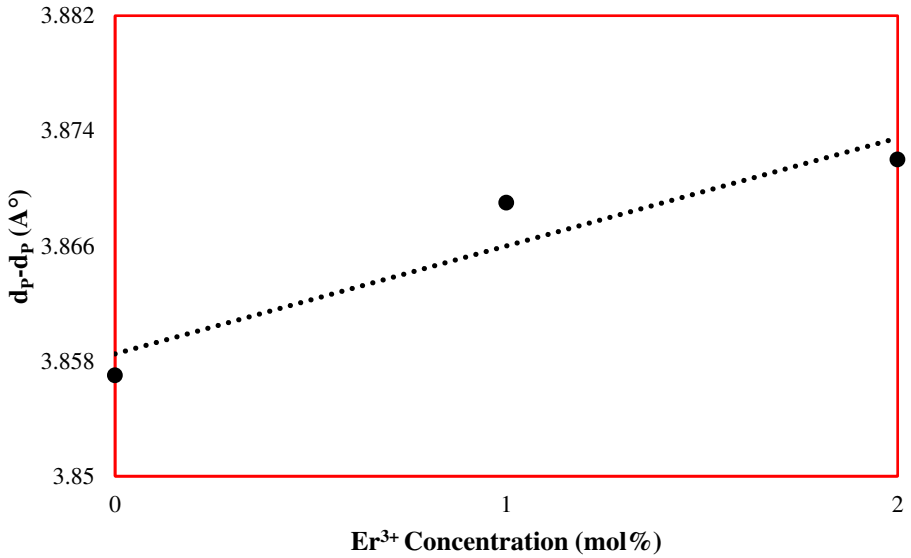

Fig 3: *The mean phosphor– phosphor separation of the studied glasses*

The observed increase in mean phosphor – phosphor separation as shown in **Figure 3** asserts that the expansion in the glass network i.e., the insertion of Er^{3+} open the glass network.

3.3.FTIR Characterization

Four clear bands were observed in the free Er^{3+} glass sample as shown in **Figure 4**. Two intense bands located at 649 and 1480 cm^{-1}, and two low intense bands centered at 785 cm^{-1} and 960 cm^{-1} are determined.

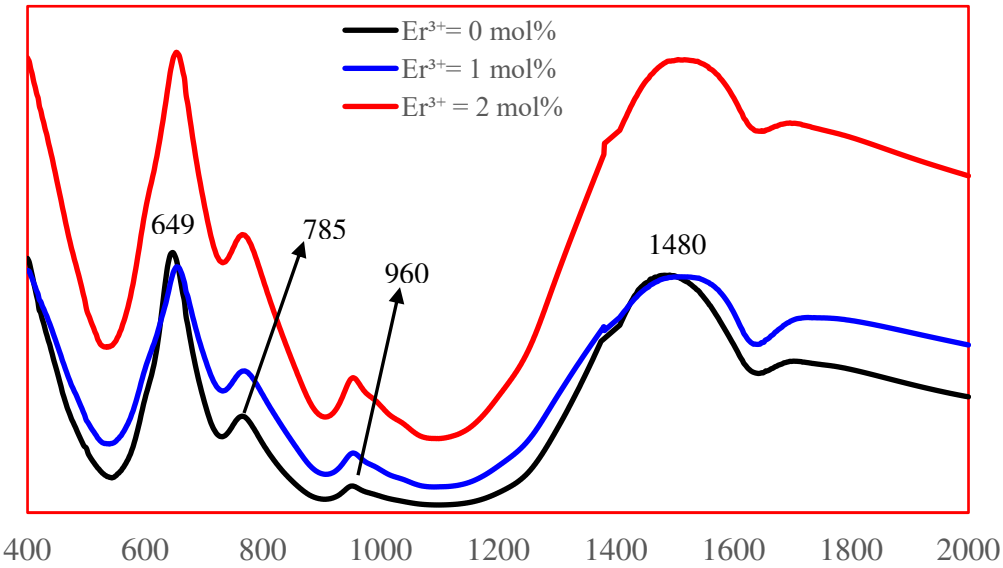

Fig 4: *FTIR spectra for undoped and Er^{3+}doped glasses*

The high intense band located at 649 cm^{-1} is attributed to the symmetric stretching modes $(P–O–P)_s$ linkages of Q^1 [11, 13, 21]. The 649 cm^{-1} band is the highest band and hence it is crossponding to the phonon energy. The present glasses have low phonon energy ranged from 649 to 656 cm^{-1} compared to the other glasses such as silicate, borate, and germanate [22-23]. The low intense band located at 785 cm^{-1} due to the asymmetric stretching modes $(P–O–P)_{as}$ linkages. The low intense band at 960 cm^{-1} indicates the existence of asymmetric stretching vibrations of PO_4^{3-} tetrahedra (P–O− ionic group). The presence of this band suggests the ionic character of all studied glasses. The broad band at 1480 cm^{-1} is assigned to the asymmetric stretching of double bonded P=O modes [11, 13, 21, 24, 25]. With the inclusion of Er^{3+}, all the peaks exhibit a slight variation to longer wavenumber and increase in the intensity. No bands were observed in the Er^{3+} doped glasses. These observations confirm the formation of NBOs due to the incorporation of Er^{3+} ions into the matrix, the increases of the degree of polymerization of the glasses, and the modifier role of the Er^{3+} ions in the studied glass network [11, 13, 21, 22, 23].

3.4.Thermal Properties

The obtained values of the glass transition temperature T_g, onset crystallization temperature T_c, and thermal stability ΔS that evaluated via the temperature gap between T_c and T_g $(T_c - T_g)$ [13] are shown in **Figure 5**. The observed decreases in T_g and increases in T_c indicate a decrease in the bonding strength of the glass structure, which in turn means the glass network somewhat less rigid. The change in Tg and T_c also linked to the number of bridging and non-bridging oxygen in the glass network. The decrease in Tg and increase in T_c mean an increase in the number of non-bridging oxygen, which indicates that the structure becomes more open. These results support the density and FTIR results. The diminution of T_g with the inceaseing of Er^{3+} concentration implies Er^{3+} enrich the glass forming ability. The thermal stability of the glass is an important factor in photonic devices, in which high values of thermal stability are desirable. Obviously, the addition of Er^{3+} improves the stability of the prepared glass. The value of $\Delta S >$ 100 ℃, which indicates that the present glasses exhibit suitable thermal stability and could be useful for photonics applications.

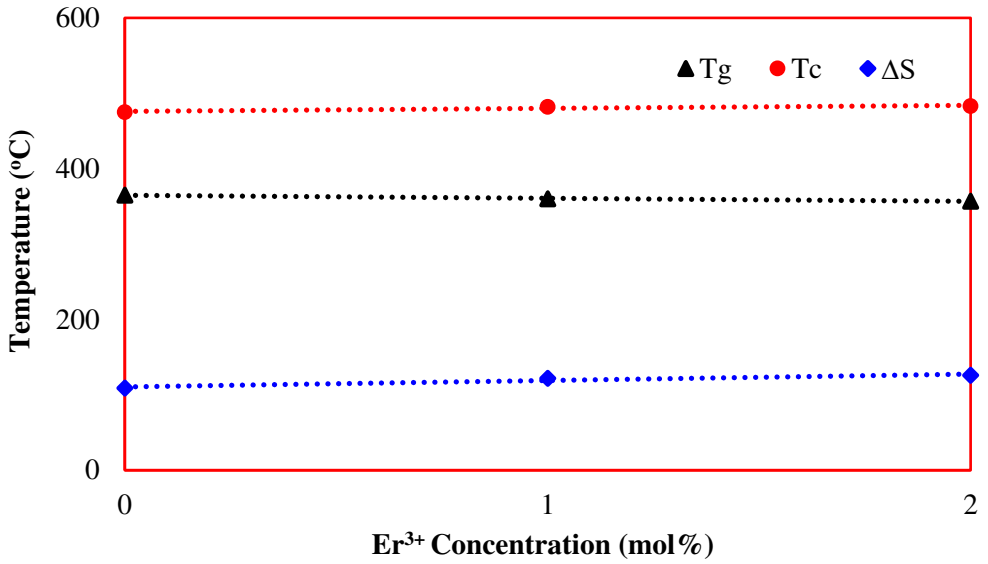

Fig 5: *T_g, T_c, and ΔS of the studied glasses*

3.5.Vickers Microhardness

The observed decrease in the Vickers microhardness with the increase of Er^{3+} as shown in **Figure 6** is attributed to the decrease in packing density. In other words, the decrease of microhardness is consistent with the weakening of glass network.

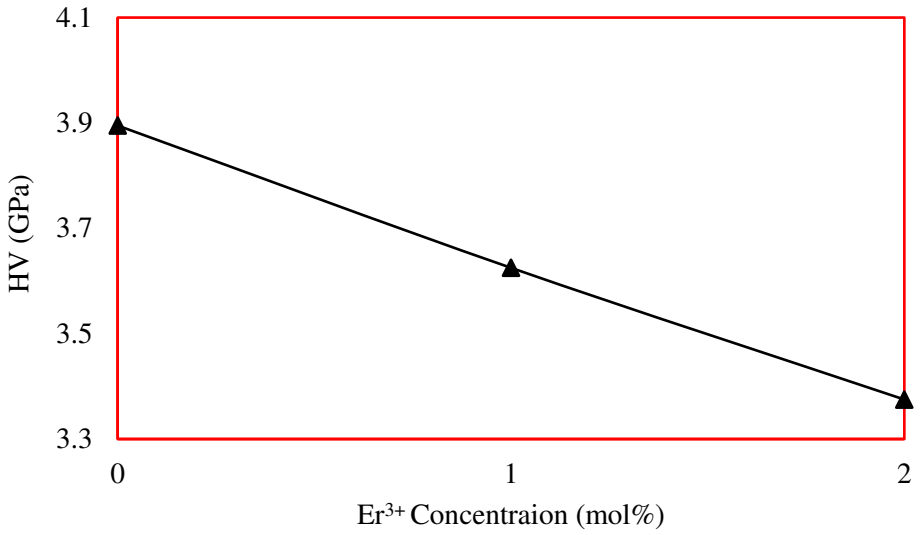

Fig 6: *Variation of microhardness with erbium ion concentratio*

3.6.Optical Prperties

The absorption coeffecient spectra of Er^{3+} free and co-doped studied glasses are displied in **Figure 7**. Nine absorption bands in the 1 mol% Er^{3+} doped samples are observed due to the various transitions in Er^{3+} ions.

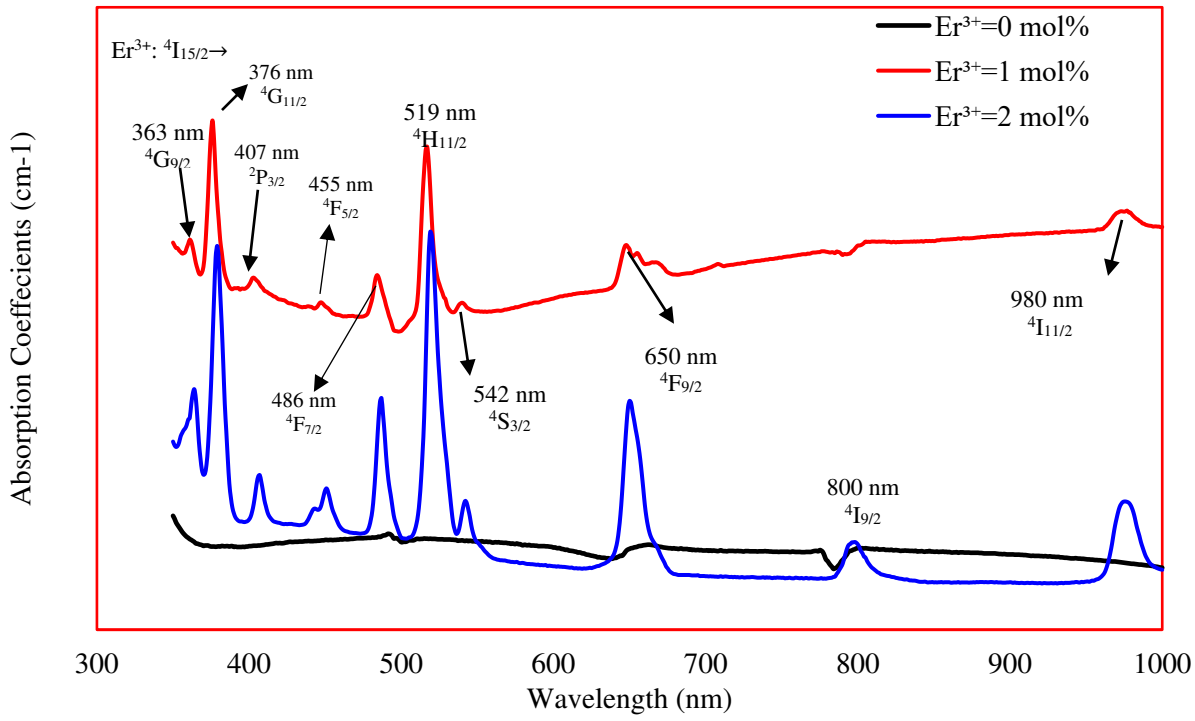

Fig 7: *Absorption spectra of studied glasses*

The absorption bands corresponding to the transitions between the Er^{3+} ion ground-state, $^4I_{15/2}$, and its various excited states belonging to the $4f^2$ configuration. The observed peaks centered at 363, 376, 407, 455, 486, 519, 542, 650, and 980 nm, these peaks were attributed to the transition from the ground state $^2I_{15/2}$ to $^4G_{9/2}$, $^4G_{11/2}$, $^4P_{3/2}$, $^4F_{5/2}$, $^4F_{7/2}$, $^4H_{11/2}$, $^4S_{3/2}$, $^4F_{9/2}$, and $^4I_{11/2}$ and transitions of Er^{3+} ions, respectively. Besides these bands, an additional band is observed at 2 mol% Er^{3+} and centered at 800 nm, which is attributed to the transition to $^4I_{9/2}$ in Er^{3+}. The longer shift in the absorption spectrum of 2 mol% indicates the glass becomes less rigidity and the increase of non-bridging oxygen atoms [17-18].

3.6.1.Optical Parameters

In semiconducting materials, during the photon absorption process for indirect band gap E_g phonon absorption or emission was stimulated. The absorption of photon energy is corresponding to $E_g - E_{ph}$, where $E_{ph} = h\omega$ represents the phonon absorption (ω is the phonon frequency). On the other hand, when the photon energy is $E_g + E_{ph}$ the photon absorption can also happen by the phonon emission, for which the absorption coefficient α is larger than that for phonon absorption. The value of E_g for indirect allowed transition deduced through solving $E_g - E_{ph}$ and $E_g + E_{ph}$ [24-25]. **Figure 8** shows the relation between of $(\alpha h\nu)^{1/2}$ versus photon energy $h\nu$ for the sample Er^{3+}free sample as a representative figure, the other samples show the same trend.

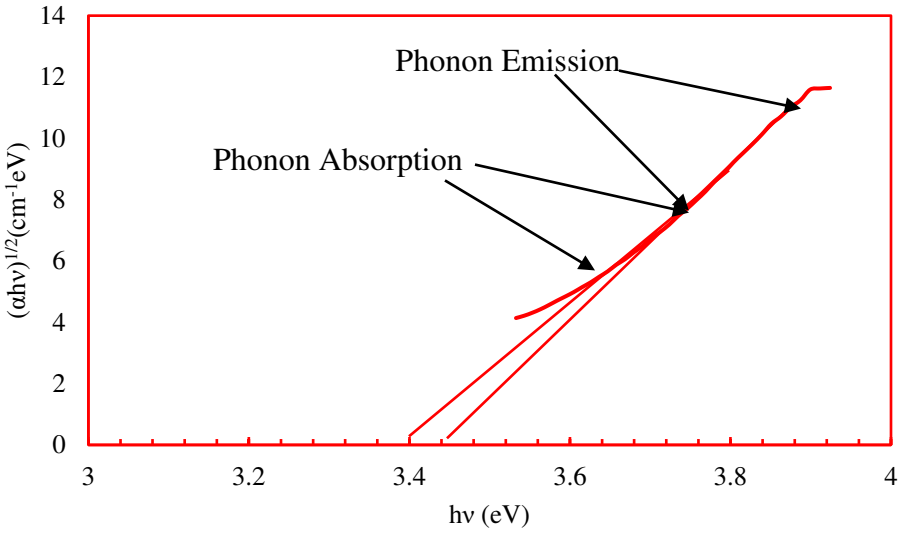

Fig 8: *Phonon absorption and emission for indirect allowed transition of the studied glasses*

The obtained values of optical band gaps versus different concentrations of Er^{3+} ions are depicted in **Figure 9**. The remarked shrank in E_g with Er^{3+} ions addition is accredited to the disruption of the bridging oxygen atoms. The inclusion of Er^{3+} creates more non-bridging oxygen

through the glass network, which augmented the disorder in the localized states of electron; thereby decreasing the donor centers causing reducing the optical band gap.

The Urbach energy E_u was calculated rely on the Urbach and Tauc's model via the relation [21]

$$\alpha\,(\nu) = \beta \exp\left(\frac{h\nu}{E_u}\right) \qquad (4)$$

where, α_o is a constant. The Urbach energy deduced through plot $\ln \alpha$ against $h\nu$ and by taking the slope of the straight line of plotted curve. The augmentation of E_u as shown in **Figure 9** indicates the increasing of the disorder in the studied glass network accredited to the imperfections formation as anomalous bond with variations in bond angle deformation, dangling bonds or NBOs in the glasses, wrong bonds besides color centers.

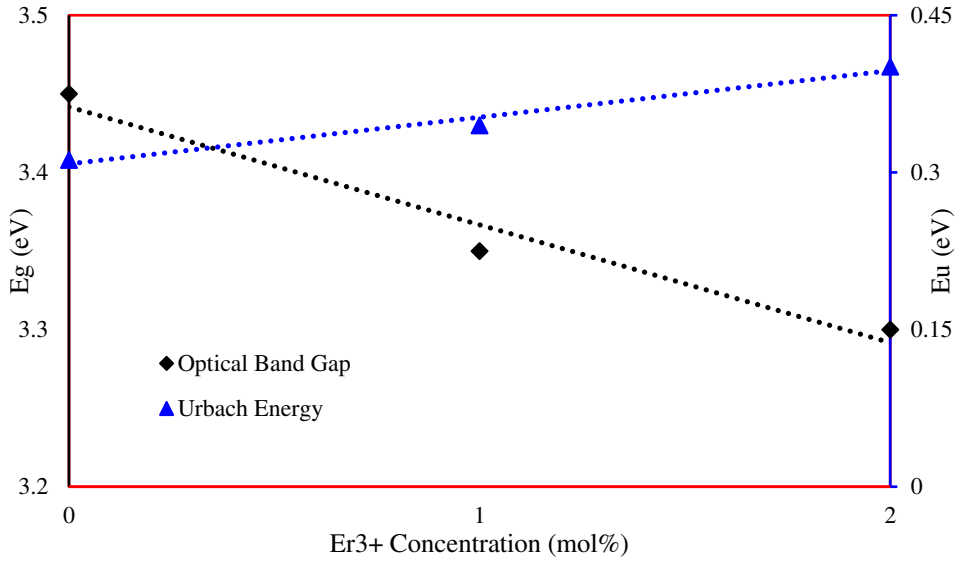

Fig 9: *Optical band gap and Urbach energy as a function in Er^{3+} of the studied glasses*

The refractive index n based optical band gap energy E_g was calculated from the equation 5 [26-27]. The obtained values of refractive indices are shown in **Figure 10**. The higher values of the refractive indices are attributed to the creation of non-bridging oxygen in the glass network. The non-bridging oxygen is much more polarizable than bridging oxygen. The glasses with a more fragmented network exhibit higher refractive indices.

$$\frac{n^2-1}{n^2+2} = 1 - \sqrt{\frac{Eg}{20}} \qquad (5)$$

The solid behavior i.e. metallic or insulator was identified through the values of metallization criterion. The metallization criterion can be valued from the relation suggested by Dimitrov and Komatsu [26-27]

$$M = 1 - \frac{n^2 - 1}{n^2 + 2} = \sqrt{\frac{E_g}{20}} \qquad (6)$$

In the present glasses, the values of metallization criterion changed from 0.415 to 0.406 as shown in **Figure 10**. The values of metallization criterion of the studied glasses are less than one. Therefore, the studied glasses have insulating nature. The studied glasses possess a metallization criterion in the 0.415–0.406, which are a good basis for nonlinear optical materials [26-27].

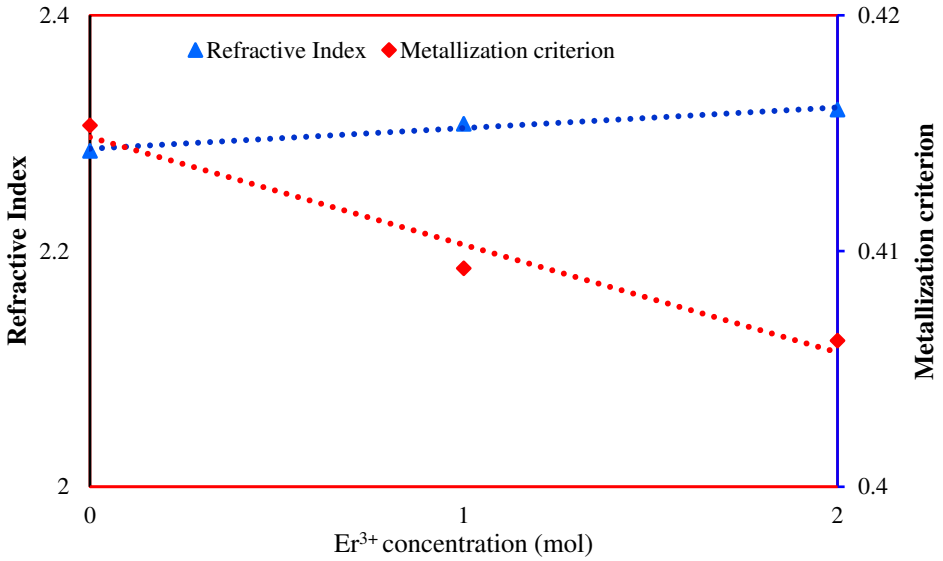

Fig 10: *Variation of refractive index and metallization criterion of the studied glasses*

3.7.Emission Spectral Analysis

Figure 11a displays the emission spectra of the studied Er^{3+} doped glasses after pumping by 320 nm. Three emission bands are observed in the blue area of the spectra and located at 446, 457, and 473 nm. The observed peaks are assigned to $^4F_{3/2} \rightarrow {}^4I_{15/2}$ (446 nm), $^2F_{5/2} \rightarrow {}^4I_{15/2}$ (457 nm) and $^4F_{7/2} \rightarrow {}^4I_{15/2}$ (473 nm) transitions. The emission intensity of 2 mol% Er^{3+} is less than 1 mol% Er^{3+} due to the concentration-quenching effect. To get more understand for the energy transfer mechanisms involved between different energy levels of Er^{3+}, the energy schematic diagram is disciplined in **Figure 11b**. The ground state electrons $^4I_{15/2}$ of Er^{3+} ions are excited to the $^2P_{3/2}$ using 320 nm excitation wavelength. The Er^{3+} ions populated at $^2P_{3/2}$ energy level then decay nonradiatively to a long-lived $^4F_{3/2}$, $^4F_{5/2}$, and $^4F_{7/2}$ levels, which is due to the multiphonon relaxation process MRP process. The electrons at $^4F_{3/2}$ are decay rapidly through radiative relaxation to the ground state $^4I_{15/2}$ level and produce blue emission peaks at 446 nm. The electrons at $^4F_{3/2}$ are also decayed through the nonradiative relaxation NR process to populate long living $^4F_{5/2}$ level.

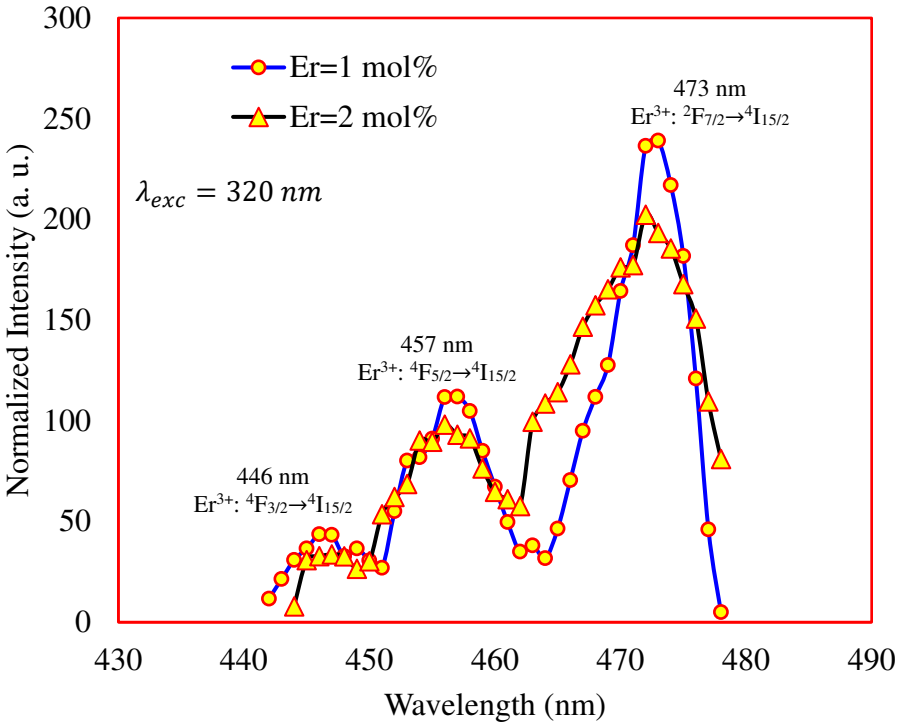

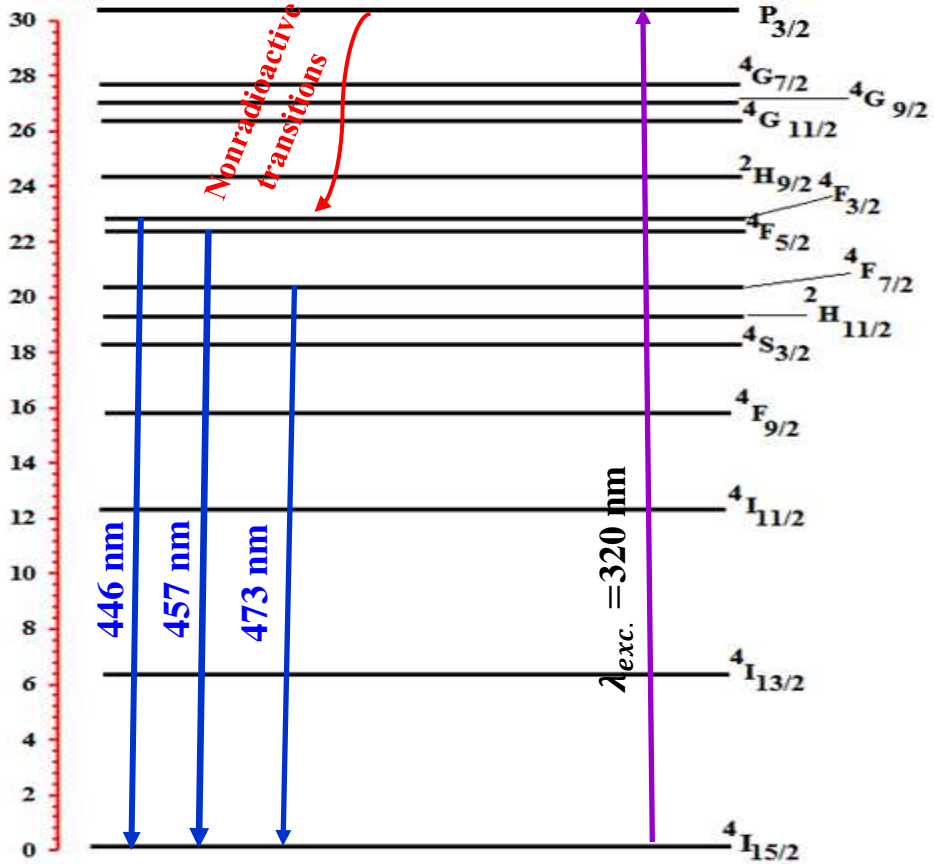

Fig 11: a) *The emission spectra and b) Transition mechanisms of* Er^{3+} *in the studied glass network*

The emission band at 457 nm is produced by radiative relaxation from $^4F_{5/2}$ level to the ground state $^4I_{15/2}$ level. The emission peak at 473 nm is produced through rapid decay of radiative relaxation from $^4F_{7/2}$ level to the ground state $^4I_{15/2}$. The CIE chromaticity coordinates for 1 and 2 mol % of Er^{3+} ion are (0.135, 0.045) and (0.133, 0.047), respectively as shown in **Figure 12**. These coordinates correspond to the blue region as shown in **Figure 12**.

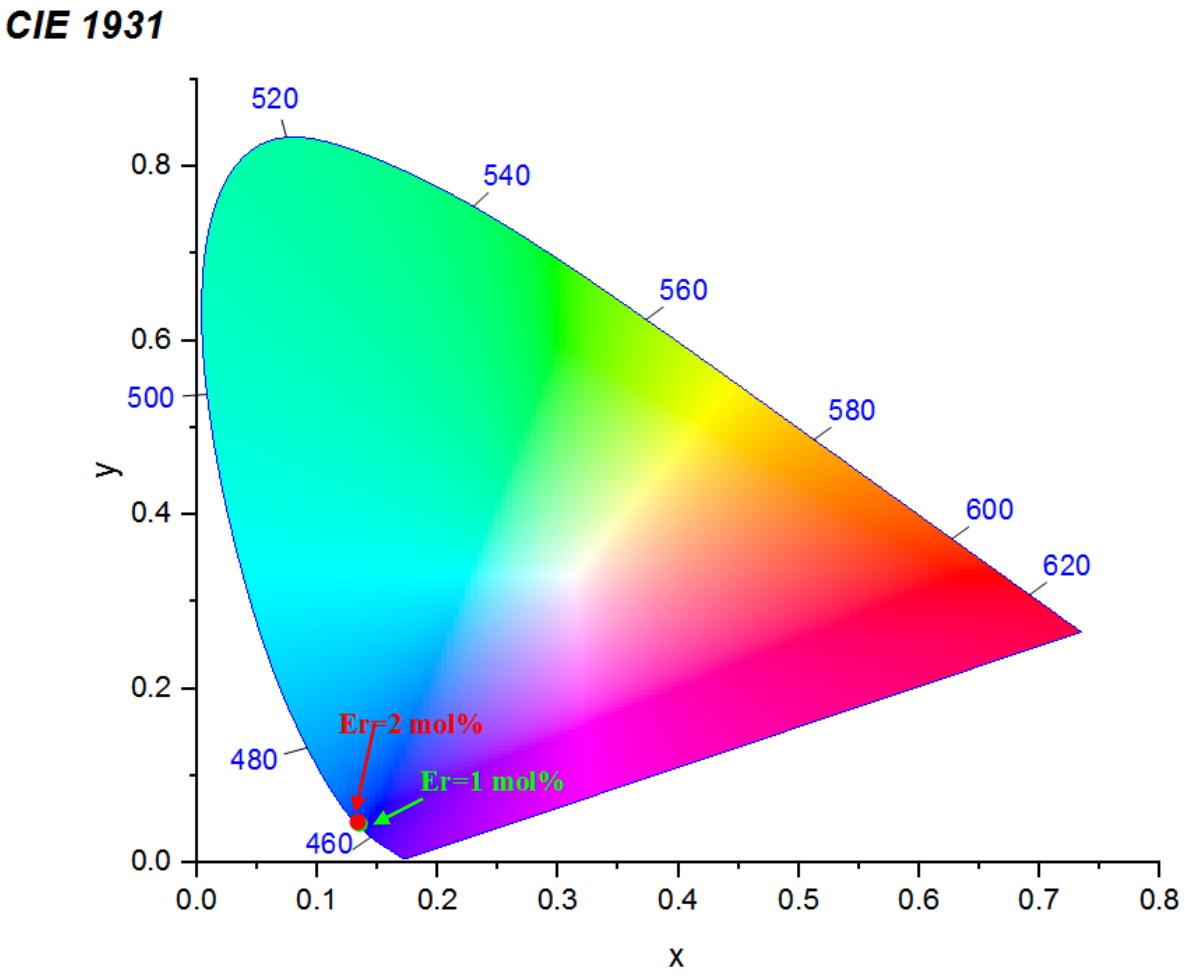

Figure 12: *CIE-1931 chromaticity diagram of the studied glasses*

4. Conclusion

Developed heavy metals oxyfluorophosphate glasses inlaid by 1 and 2 mol % of Er^{3+} ions were prepared. The obtained results of density, FTIR, thermal properties, Vickers microhardness, optical band gap, Urbach energy, and refractive index are in perfect tune with each other. The structural properties showed that Er^{3+} ions act as a modifier role in the present glass network. The studied glass network is an open structure and many non-bridging oxygen atoms were created in the glass network. The studied glasses have low phonon energy ranging from 649

to 656 cm^{-1}. The present glasses have high thermal stability. Under 320 nm excitation wavelength, three bands in the blue region centered at 446, 457, and 473 nm were generated. Hence, the reported glasses are potentially usable as photonic materials, especially as a blue emitter.

References

1.Chen Shi, Yanan Zhu, Gaofeng Zhu, Xiuyu Shen, and Mingqiao Ge, "*Phototunable full-color emission of dynamic luminescence materials"*, Journal of Materials Chemistry C, 6 (2018) 9552-9560.

2.Dengfeng Li, Jie Wang, and Xiang Ma, "*White-light-emitting materials constructed from supramolecular approaches*", Advanced Engineering Materials, 6 (2018) 1-27.

3.K. Annapoorani, K. Maheshvaran, S. Arunkumar, N. Suriya Murthy, and K. Marimuthu1, *"Structural and luminescence behavior of Er^{3+} ions doped barium tellurofluoroborate glasses",* Luminescent Materials, 135(25) (2015) 1090-1098.

4.Changming Xia, Jiantao Liu, Wei Zhang, Wanting Liang, Ying Han, Jinhui Yuan, and Guiyao Zhou, *"$Yb^{3+}/Tm^{3+}/Ho^{3+}$ tri-doped silica-based glass: intense up-conversion and broad near-infrared emission",* Optical and Quantum Electronics, 48 (2016) 257.

5.Ch. Basavapoornima, C. R. Kesavulu, T. Maheswari, Wisanu Pecharapa, Shobha Rani Depuru, and C. K. Jayasankar, *"Spectral characteristics of Pr^{3+}-doped lead based phosphate glasses for optical display device applications",* Journal of Luminescence, 227 (2020) 117585, 2020.

6.Ryszard S Romaniuk, "*Non-linear glasses and metaglasses for photonics, a review: Part II. Kerr nonlinearity and metaglasses of positive and negative refraction*", 6937(1) (2007) 1-14.

7.Yu Zhang, Hao Lei, Guannan Li, Lingwei Zeng, and Jianfeng Tang, *"Yb^{3+}/Er^{3+} co-doped transparent tellurite glass-ceramic for enhanced upconversion luminescence",* Optical Materials, 99 (2020) 11-20.

8.Sha Jiang, Peng Zeng, Liqing Liao, Shifeng Tian, Hai Guo, Yonghu Chen, Changkui Duan, and Min Yin*, "Optical thermometry based on upconverted luminescence in transparent glass ceramics containing $NaYF_4:Yb^{3+}/Er^{3+}$ nanocrystals",* Journal of Alloys and Compounds, 617 (2014) 538-541.

9.Chengguo Ming, Liqun An, and Xiaobin Ren,*"Investigation on $Yb^{3+}/Er^{3+}/Tm^{3+}$ tri-doped phosphate glass ceramic for white-light-emitting diode",* Applied Optics, 51(16) (2012) 3190-3193.

10. M. A. Marzouk, S. M. Abo-Naf, H. A. Zayed, and N. S. Hassan, " *Glass former effects on photoluminescence and optical properties of some heavy metal oxide glasses doped with transition metal ions",* Journal of Applied Spectroscopy, 84(1) (2017) 162-169.

11. Marta Kuwik, Joanna Pisarska, and Wojciech A. Pisarski, *"Influence of oxide glass modifiers on the structural and spectroscopic properties of phosphate glasses for visible and near-infrared photonic applications"*, Materials, 13 (2020) 1-20.

12. Gustavo Galleani, Silvia Helena Santagneli, Yannick Ledem, Younès Messaddeq, Oliver Janka, Rainer Pöttgen, and Hellmut Eckert, *"Ultraviolet upconversion luminescence in a highly transparent triply-doped Gd^{3+}–Tm^{3+}–Yb^{3+} fluoride–phosphate glasses"*, The Journal of Physical Chemistry C, 122(4) (2018) 2275–2284.

13. M. Deepa, Ramachari Doddoji, A. V. Chandrasekhar, *"Structural and optical properties of Sm^{3+}-doped borate glasses for luminescent applications",* Optical and Quantum Electronics, 51 (2019) 395.

14. M. Naftaly and A. Jha, *"Nd^{3+}-doped fluoroaluminate glasses for a 1.3um amplifier,"* Journal of Applied Physics, 87 (2000) 2098-2104.

15. Aly Saeed, Y. H. Elbashar, and S. U. El Kameesy, "*Optical spectroscopic analysis of high density lead borosilicate glasses"*, Silicon, 10 (2018) 185-189.

16. Maria Bosca, Lidia Pop, Gheorghe Borodi, Petru Pascuta, and Eugen Culea, *"XRD and FTIR structural investigations of erbium-doped bismuth–lead–silver glasses and glass ceramics",* Journal of Alloys and Compounds, 479 (2009) 579–582.

17. Diego Pugliese, Nadia G. Boetti, Joris Lousteau, Edoardo Ceci-Ginistrelli, Elisa Bertone, Francesco Geobaldo, and Daniel Milanese, "*Concentration quenching in an Er-doped phosphate glass for compact optical lasers and amplifiers*", Journal of Alloys and Compounds, 657 (2016) 678-683.

18. Hongtao Sun, *Shiqing* Xu, Shixun Dai, Lei Wen, Junjie Zhang, Lili Hu, and Zhonghong Jiang, "*Efficient frequency upconversion emission in Er^{3+}-doped novel strontium lead bismuth glass",* Journal of Non-Crystalline Solids, 351 (2005) 288–292.

19. Rajeshree Patwari and B. Eraiah, "*Optical and plasmonic properties of Er^{3+} and silver co-doped borate nano-composite glasses"*, Materials Research Express, 6(11) (2019) 1-31.

20. Aly Saeed, Y. H. Elbashar, and S. U. El Khameesy, "*A novel barium borate glasses for optical applications"*, Silicon, 10 (2018) 569–574.

21. A. M. El-Batala, Aly Saeed, N. Hendawy, M. M. El-Okr, and M.K. El-Mansy, "*Influence of Mo or/and Co ions on the structural and optical properties of phosphate zinc lithium glasses*", Journal of Non-Crystalline Solids, 559 (2021) 120678.

22. Doris Möncke and Hellmut Eckert, "*Review on the structural analysis of fluoride-phosphate and fluorophosphate glasses"*, Journal of Non-Crystalline Solids: X, 3 (2019) 1-15.

23. Kohei Yoshimoto, Atsunobu Masuno, Motoi Ueda, Hiroyuki Inoue, Hiroshi Yamamoto, and Tastunori Kawashima, "*Low phonon energies and wideband optical windows of La_2O_3-Ga_2O_3 glasses prepared using an aerodynamic levitation technique*", Scientific Reports, 7(1) (2017) 1-9.

24. H. Y. Morshidy and M. S. Sadeq, "*Influence of cobalt ions on the structure, phonon emission, phonon absorption and ligand field of some sodium borate glasses*", Journal of Non-Crystalline Solids, 525 (2019) 1-6.

25. M. S. Sadeqa and H. Y. Morshidy, "*Effect of mixed rare-earth ions on the structural and optical properties of some borate glasses"*, Ceramics International, 45 (2019) 18327–18332.

26. Yanling Wang, Shixun Dai, Feifei Chen, Tiefeng Xu, and Qiuhua Nie, "*Physical properties and optical band gap of new tellurite glasses within the TeO_2–Nb_2O_5–Bi_2O_3 system*", Materials Chemistry and Physics, 113 (2009) 407–411.

27. Aly Saeed, Y. H. Elbashar, R. M. El shazly, *"Optical properties of high density barium borate glass for gamma ray shielding applications"*, Optical and Quantum Electronics, 48 (2016) 1.

Figures

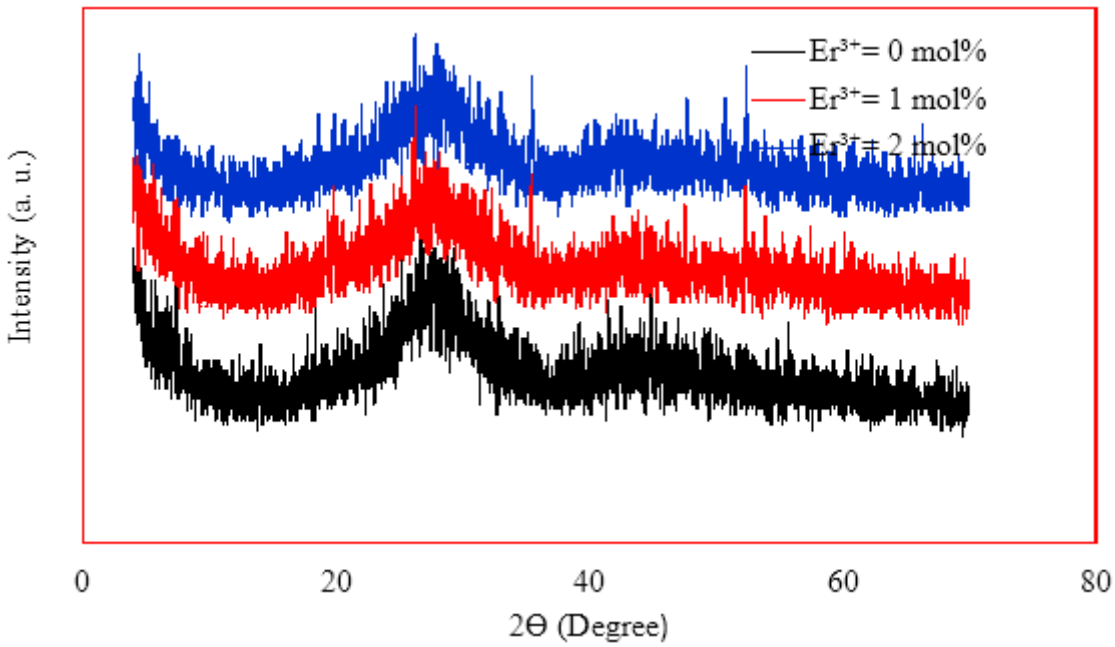

Figure 1

X-ray diffraction patterns for the studied materials

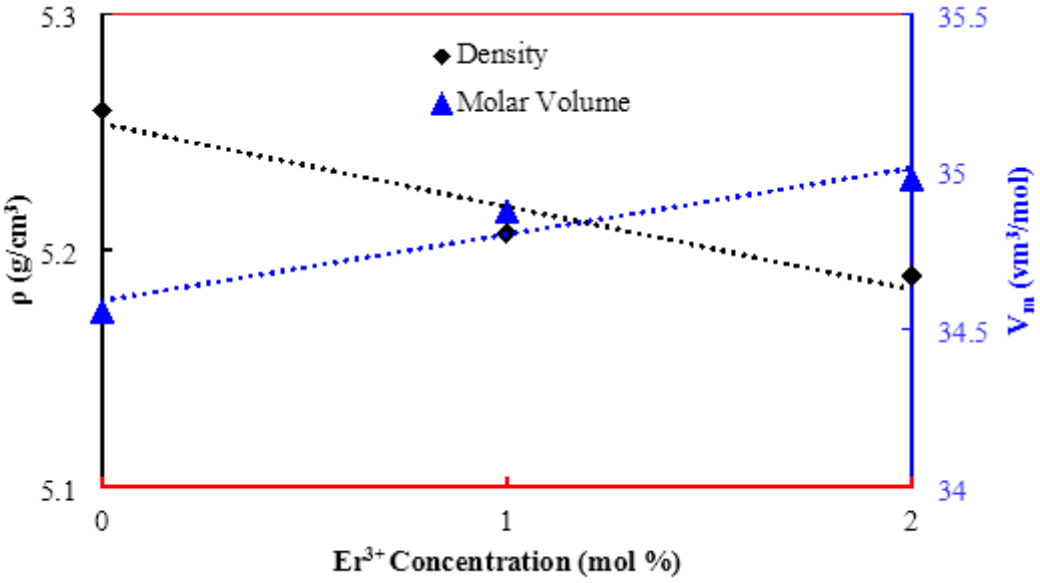

Figure 2

The obtained results of density and molar volume of the studied glasses

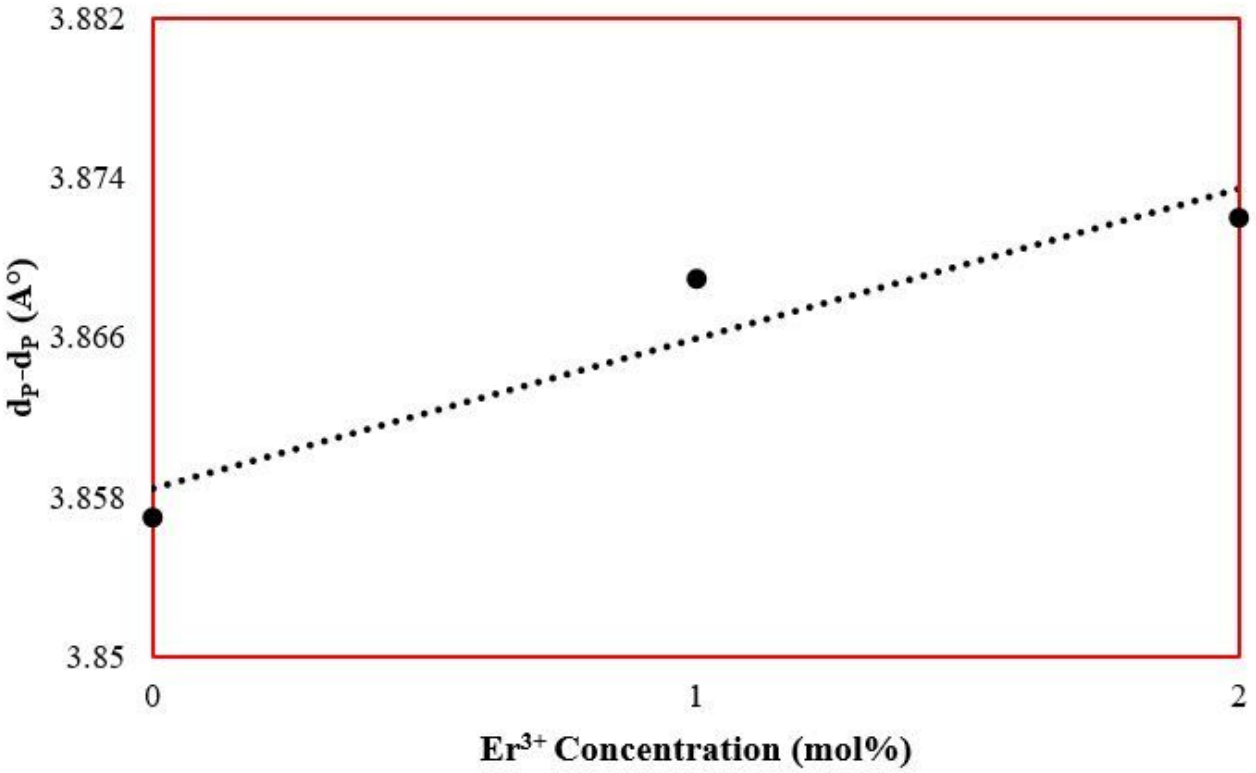

Figure 3

The mean phosphor– phosphor separation of the studied glasses

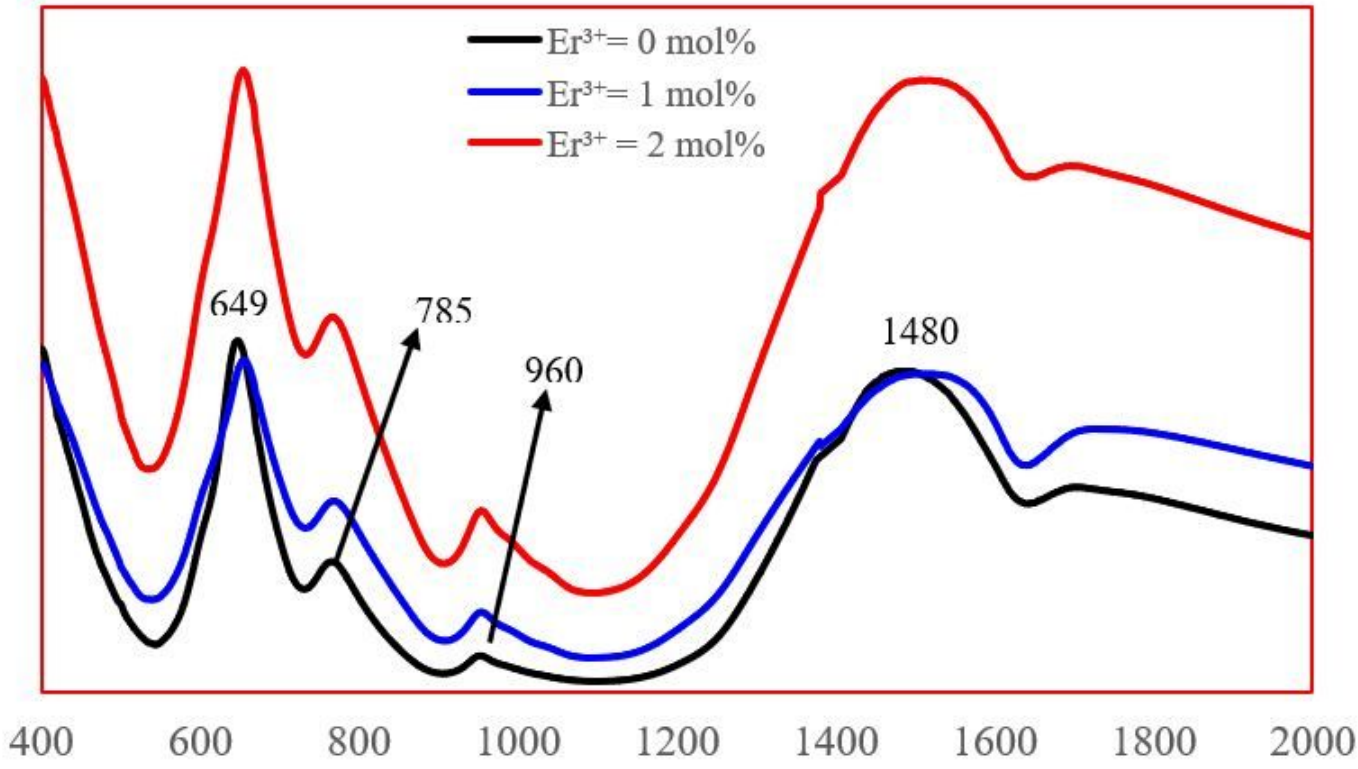

Figure 4

FTIR spectra for undoped and Er3+doped glasses

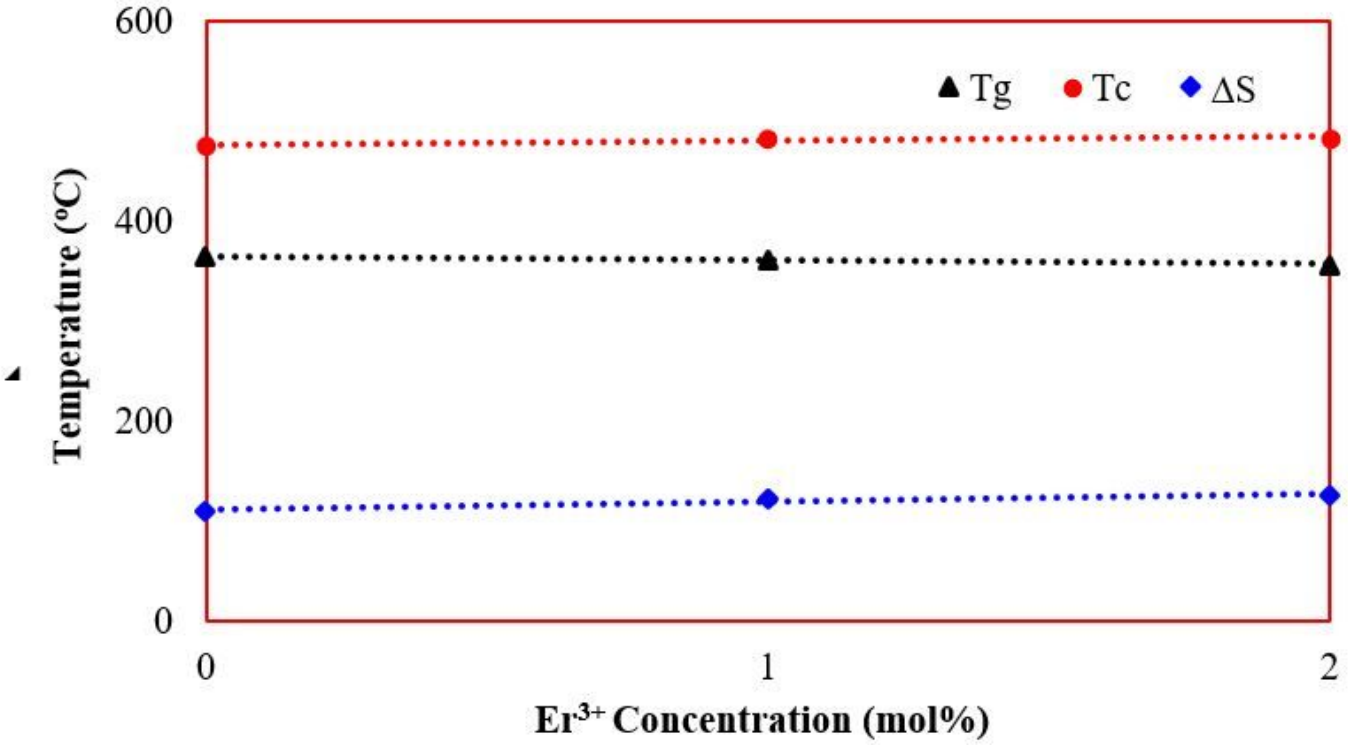

Figure 5

T_g, T_c, and ΔS of the studied glasses

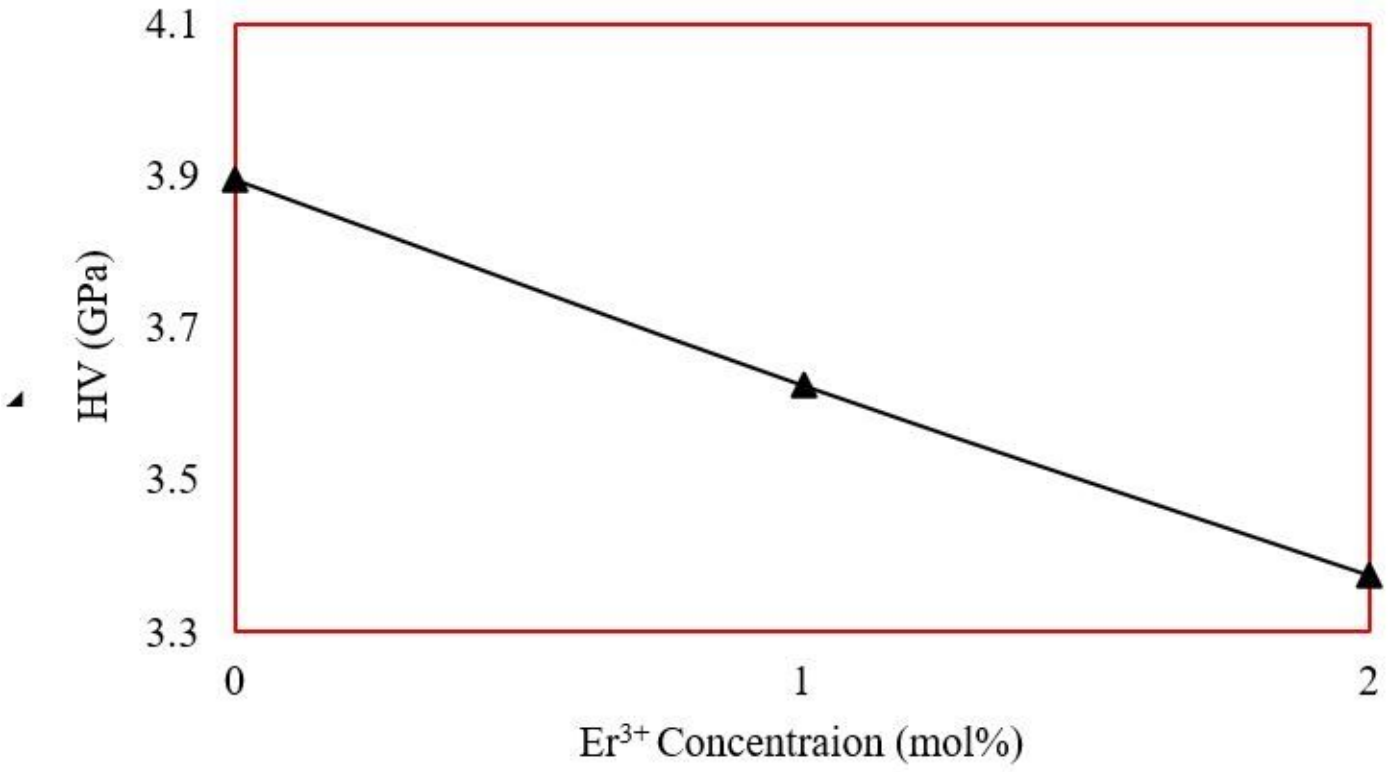

Figure 6

Variation of microhardness with erbium ion concentratio

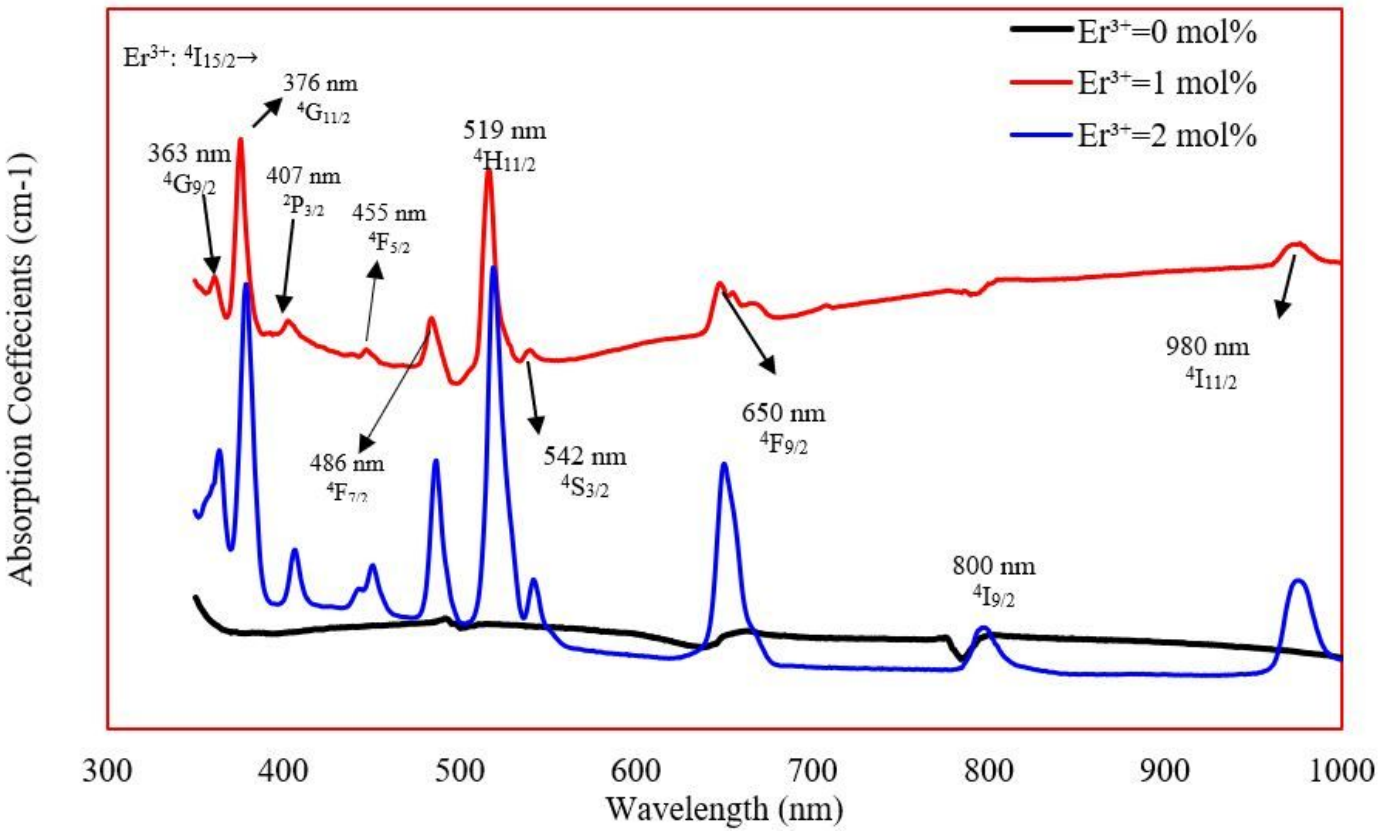

Figure 7

Absorption spectra of studied glasses

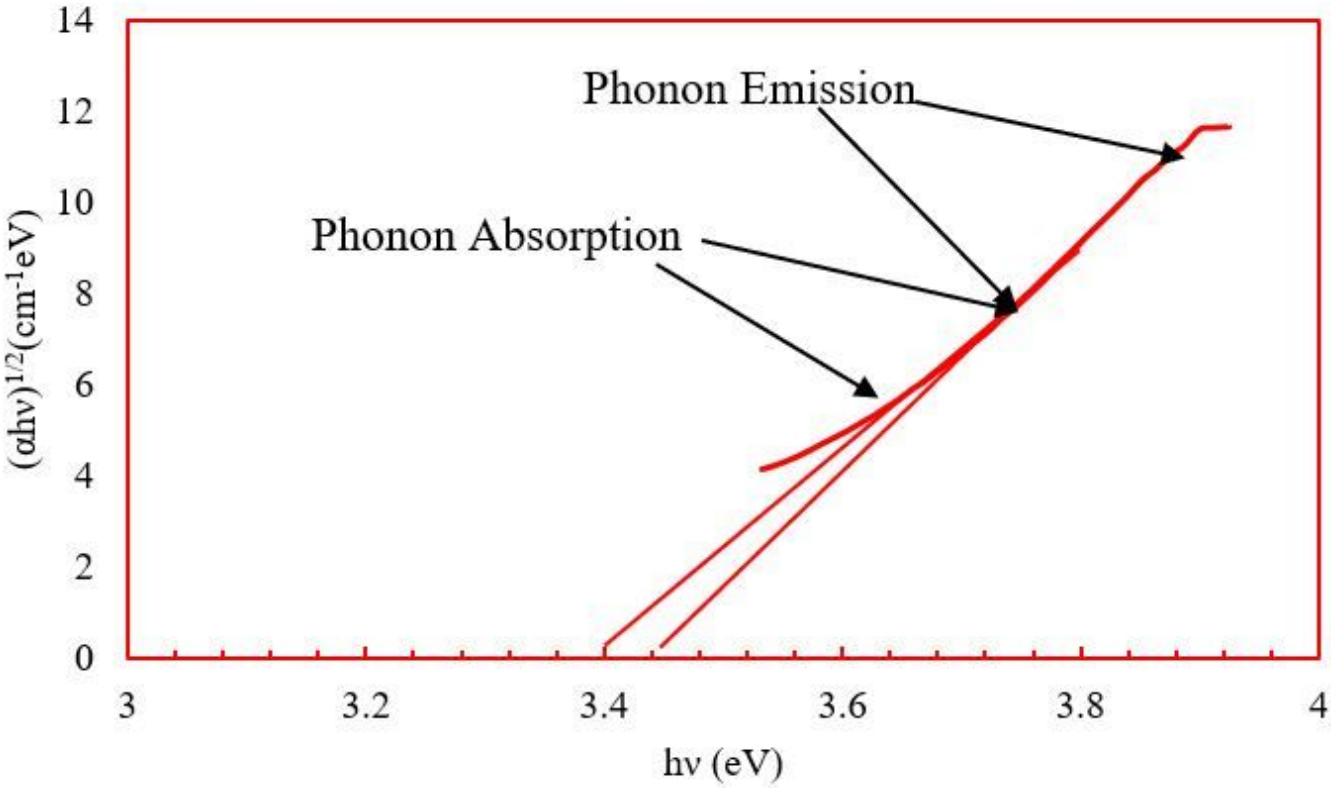

Figure 8

Phonon absorption and emission for indirect allowed transition of the studied glasses

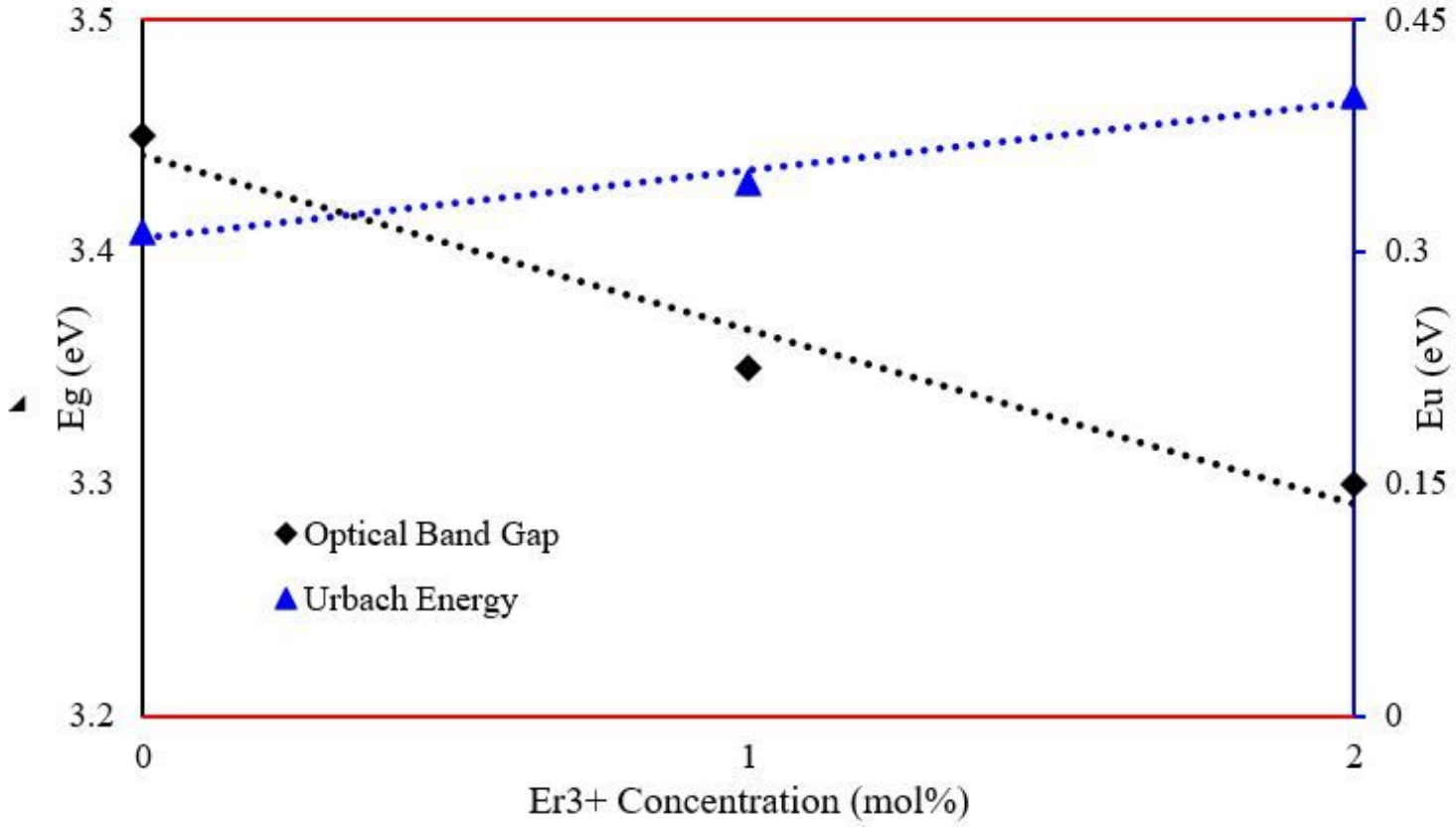

Figure 9

Optical band gap and Urbach energy as a function in Er3+ of the studied glasses

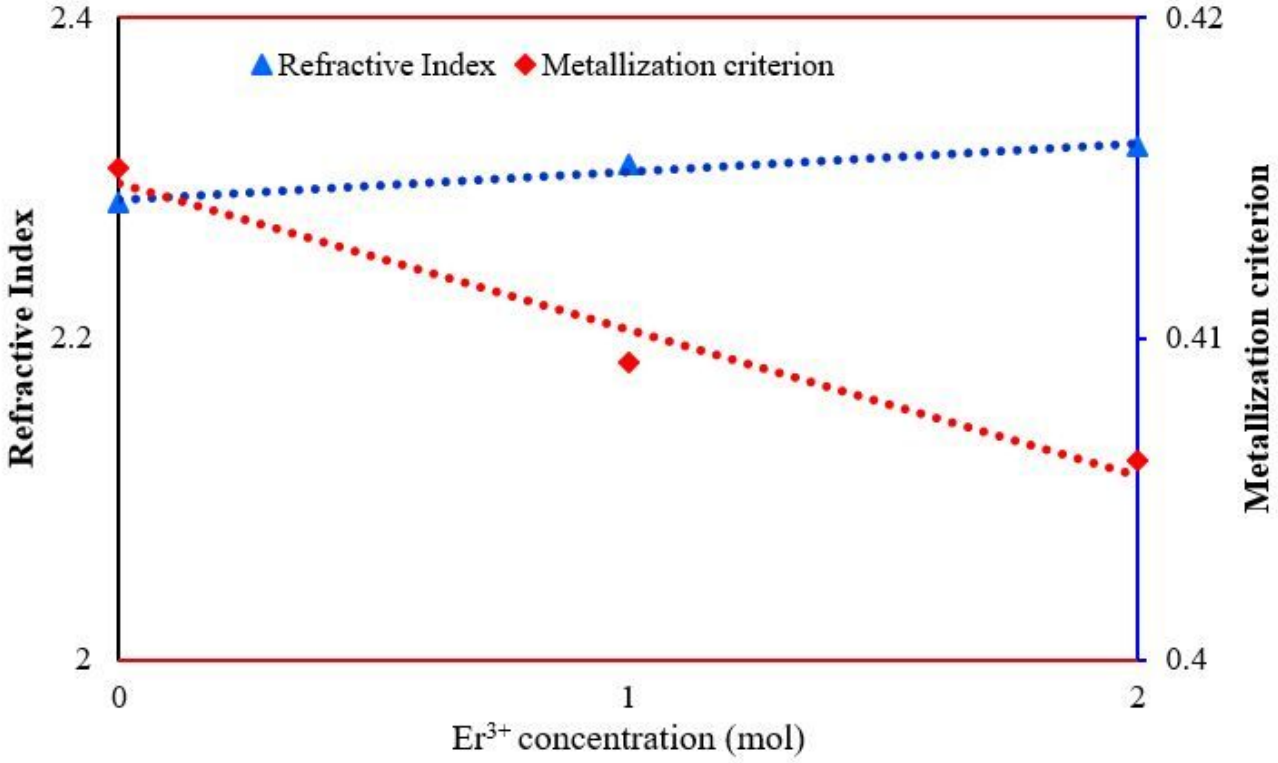

Figure 10

Variation of refractive index and metallization criterion of the studied glasses

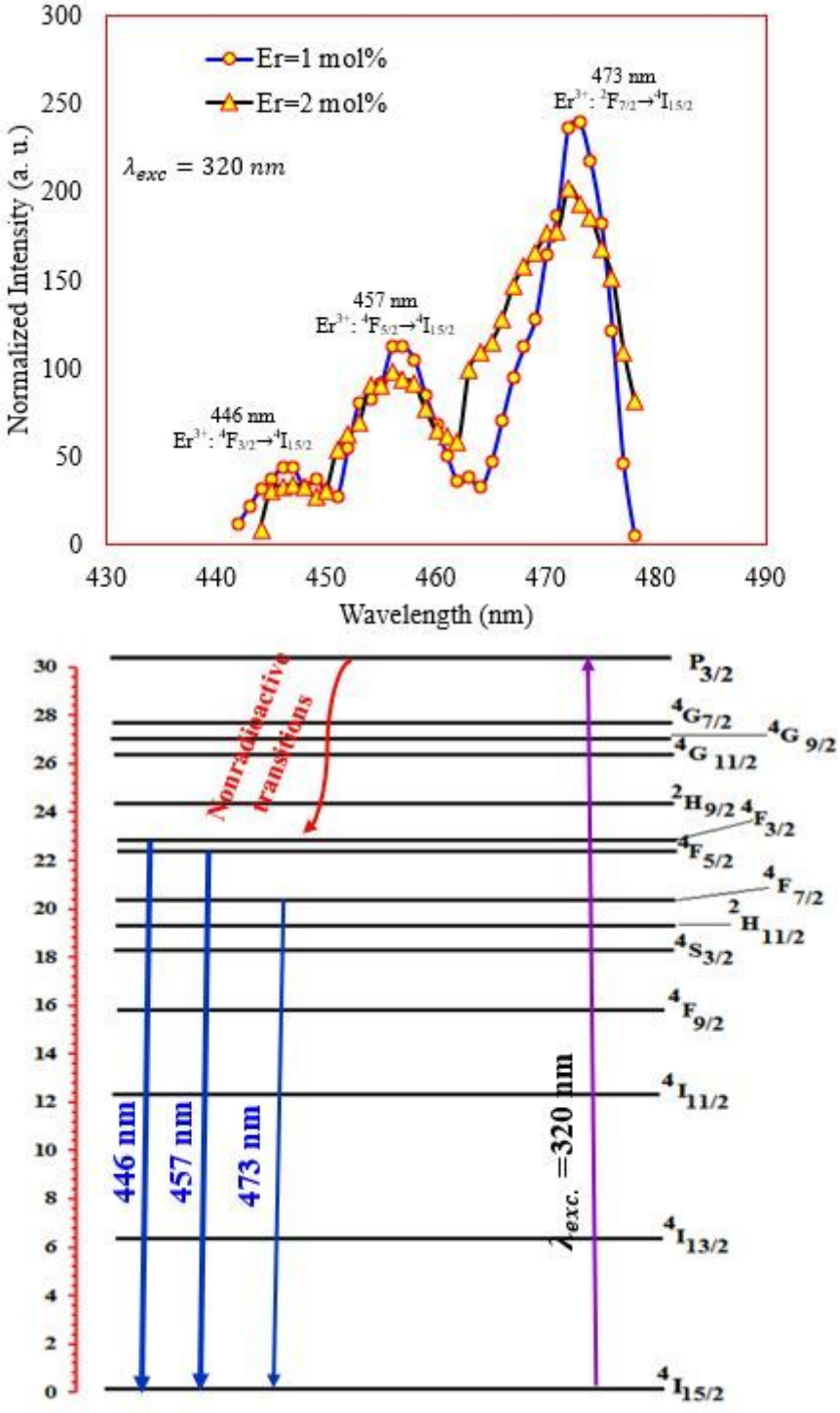

Figure 11

a) The emission spectra and b) Transition mechanisms of Er3+ in the studied glass network

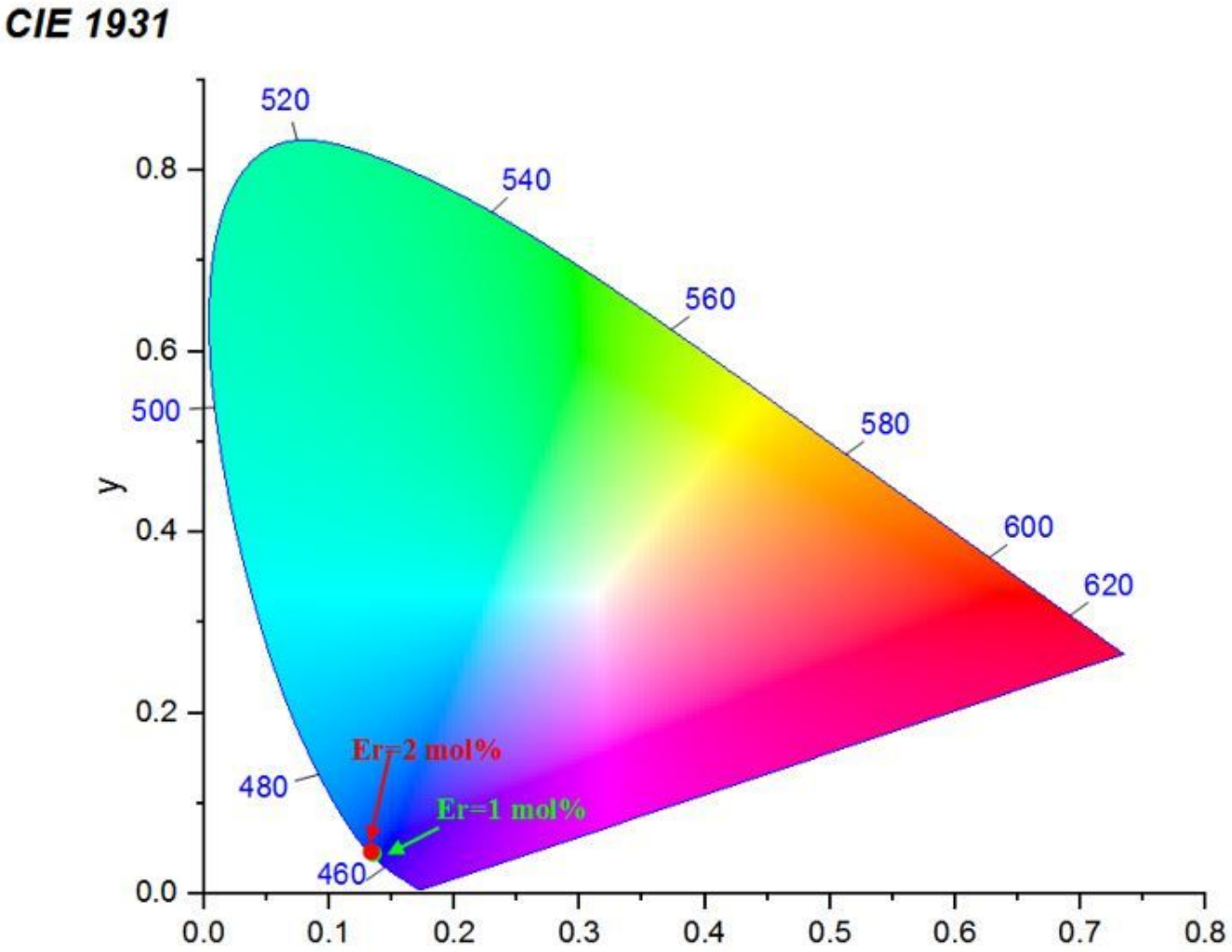

Figure 12

CIE-1931 chromaticity diagram of the studied glasses